Conference on Modelling Fluid Flow (CMFF'25)
The 19th International Conference on Fluid Flow Technologies
Budapest, Hungary, August 26 - August 29, 2025

DEVELOPMENT OF A CYLINDRICAL-BLADE WIND TURBINE DRIVEN BY A NECKLACE VORTEX

Tsutomu TAKAHASHI[1], Ryuga SADAOKA[2], Yasunori SATO[3]

[1] Corresponding Author. Department of Mechanical Mechanics, Faculty of Engineering, Nagaoka University of Technology. 1603-1 Kamitomioka, Nagaoka, Niigata. 940-2188 Japan. Tel.: +81 258 47 9728, E-mail: ttaka@nagaokaut.ac.jp
[2] Department of Mechanical Mechanics, Graduate School of Nagaoka University of Technology. E-mail: s213027@stn.nagaokaut.ac.jp
[3] Department of Mechanical Mechanics, Faculty of Engineering, Nagaoka University of Technology. E-mail: yasusato@nagaokaut.ac.jp

ABSTRACT

When the blade of a horizontal-axis wind turbine is replaced with a circular cylinder and a ring plate is installed downstream, a necklace vortex forms at their intersection. As the cylinder rotates, this vortex remains stationary on the opposite side of its motion, generating lift and driving the turbine. This is known as a necklace vortex-driven cylinder-blade wind turbine. Developed by the authors, this turbine rotates at less than 1/20th of the peripheral speed of conventional blade-type turbines while generating over ten times the torque. Its low speed eliminates noise and vibration, and the soft-material cylinder blades enhance safety, making it suitable for installation near human living spaces. The turbine consists of a single cylinder as the blade and a ring plate positioned in its wake. Key design parameters include the cylinder's diameter and length, the ring plate's diameter and radial width, and their spacing. This presentation examines how these factors influence power characteristics.

Keywords: cylindrical blade, horizontal axis wind turbine, necklace vortex, vertical vortex

NOMENCLATURE

C_P	[-]	power coefficient
d	[mm]	diameter of cylinder blade
D	[mm]	diameter of ring plate
F_L	[N]	lift force on cylinder blades
L	[mm]	length of cylinder blade
n	[rpm]	rotational speed of blades
N	[-]	number of blades
s	[mm]	gap between blade and ring plate
T	[Nm]	Torque acting on rotating shaft
U	[m/s]	wind velocity
W	[mm]	width of ring plate

Subscripts and Superscripts

max maximum value a series of measurements

1. INTRODUCTION

When a cylindrical bluff body is placed in a uniform flow, periodic shedding of Kármán vortices from both sides generates fluctuating lift forces. If the shedding frequency matches the natural frequency of the structure, resonance can occur, leading to large-amplitude oscillations that may damage the structure. To suppress such wake instabilities and vortex shedding, Rashidi et al. [1] systematically reviewed existing control strategies

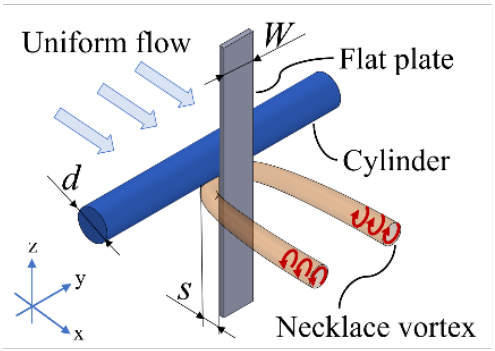

Figure 1. Longitudinal vortices at cross-section of cruciform system with cylinder and flat plate.

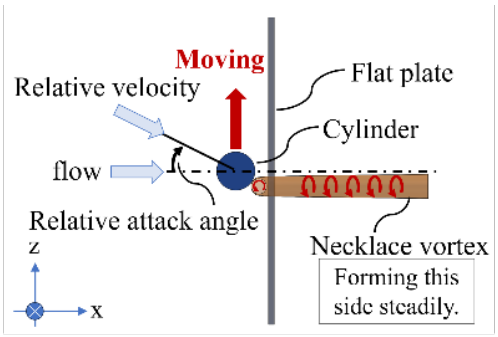

Figure 2. Mechanism of lift force generation by Necklace vortex.

and classified them into two categories: **active control** and **passive control**. Active control involves manipulating the flow using external energy, while passive control modifies the flow without external input by changing the geometry of the body or attaching devices such as splitter plates[2-5]. Passive control is generally simpler in structure and easier to implement, making it more practical for engineering applications [6].

Our group has developed a passive control method to suppress Kármán vortex-induced excitation by placing a secondary circular cylinder downstream in a cruciform arrangement [7,8]. Experiments revealed that this configuration not only reduces oscillation amplitude but can also induce vibrations in the upstream cylinder. Two types of longitudinal vortices—trailing vortex (TV) and necklace vortex (NV)—were observed near the intersection, depending on the gap ratio (s/d). Kato et al. [9] later replaced the downstream cylinder with a strip plate, which proved more effective in enhancing resonant vibrations. This concept was further applied to develop a micro power generator utilizing longitudinal vortex-induced vibration (LVIV) [10].

Longitudinal vortices, with their rotational axis aligned with the flow direction, are periodically generated in the cylinder-plate system shown in Figure 1, which consists of a crossed arrangement with a prescribed gap in uniform flow. As shown in Figure 2, when the cylinder moves parallel to the plate, a relative angle of attack is introduced, disrupting the periodicity of the necklace vortex and localizing it on the opposite side of the cylinder's motion. At this point, a steady lift force acts on the cylinder due to the reaction force of the suction flow at the front of the cylinder, induced by the necklace vortex [11].

The longitudinal vortex-driven cylindrical blade wind turbine is a novel wind turbine concept in

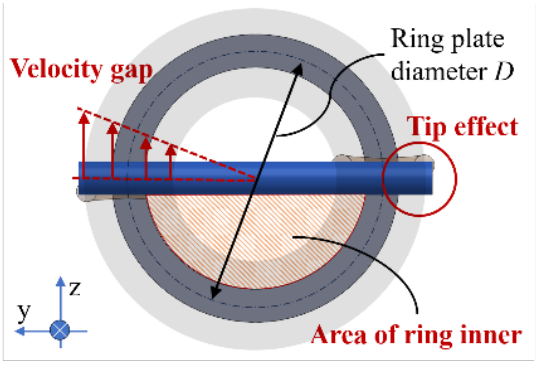

FIGURE 3. DIFFERENCE DUE TO THE CURVATURE GIVEN TO THE FLAT PLATE.

which a rotating shaft is attached to the cylinder as a blade, driven by the necklace vortex flowing through the gap between the ring plate and the trailing edge of the cylinder [12]. However, the effects of this phenomenon have not been fully considered in practical wind turbine systems (Figure 3). Sakamoto et al. demonstrated that varying the ring plate width W for a given cylindrical blade diameter d influences performance and that an optimal face width ratio exists [13].

Therefore, this study aims to clarify the effect of curved flats on performance characteristics and propose a method for predicting wind turbine performance based on geometric parameters.

2. EXPERIMENTAL APPARATUS AND METHODS

Figure 4 shows the experimental apparatus and each parameter. The apparatus was set up in a wind tunnel with a test section of 320 mm × 320 mm × 1000 mm. The center diameter D of the ring plate was varied for different combinations of the cylindrical blade diameter d and the ring plate width W, while maintaining a constant wind velocity U.

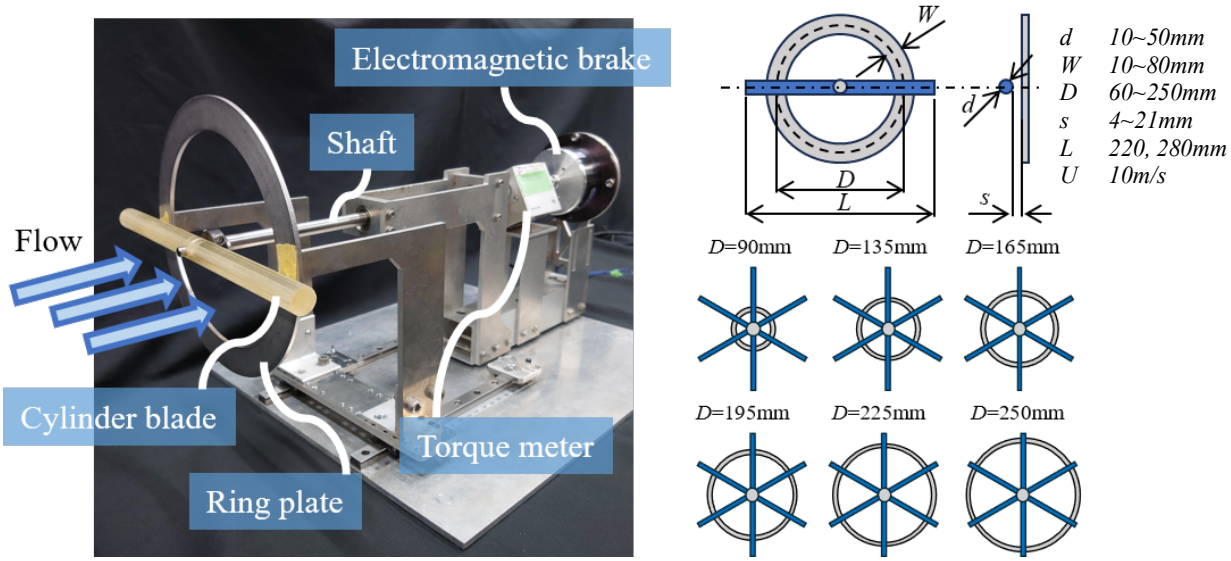

Figure 4. Schematic of wind turbine device and each parameter.

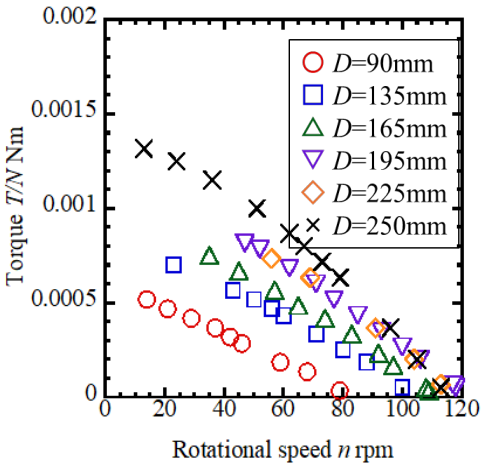

(a) Rotational speed vs. Torque

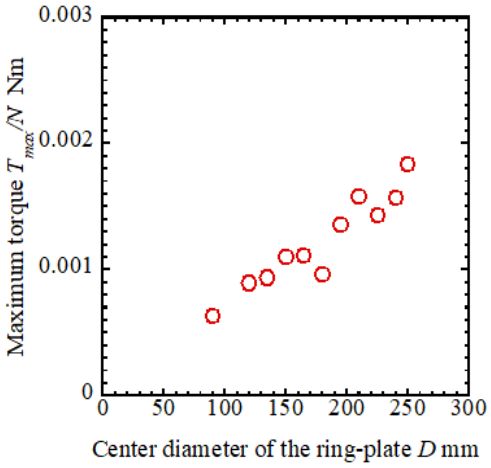

(b) Center diameter of the ring-plate vs. Maximum torque

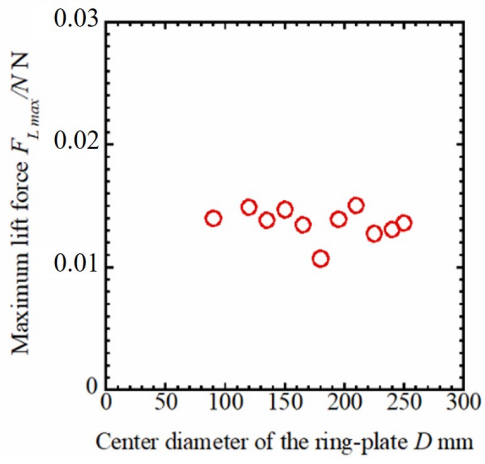

(c) Center diameter of the ring-plate vs. Maximum lift force

Figure 5. Effect of ring plate diameter *D* on the measured torque and lift per blade. (*d*=10mm, *W*=10mm, *s*=4mm, *L*=280mm, *N*=6, *U*=10m/s)

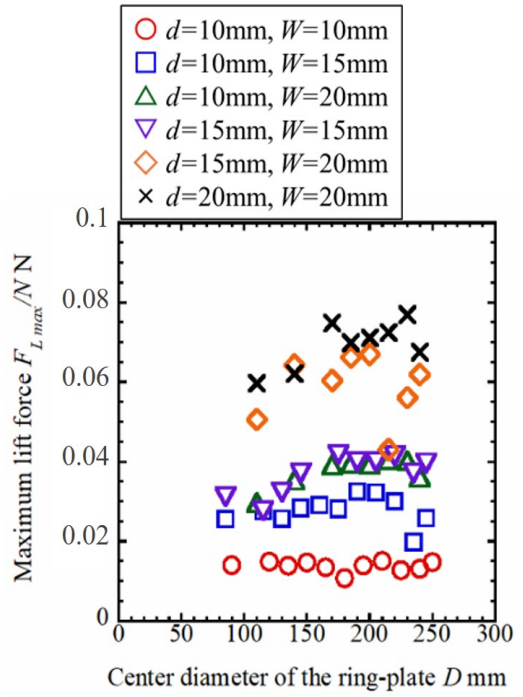

Figure 6. Relationship between the ring plate diameter and the maximum lift force for various cylinder blade diameters and ring plate widths (*L*=280mm, *s*=4-7mm, *U*=10m/s, *N*=2-6).

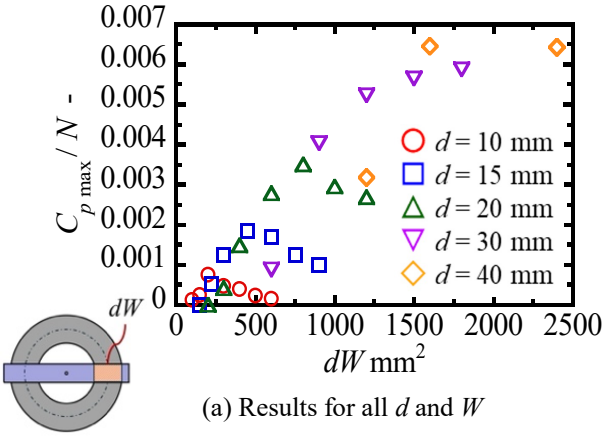

(a) Results for all *d* and *W*

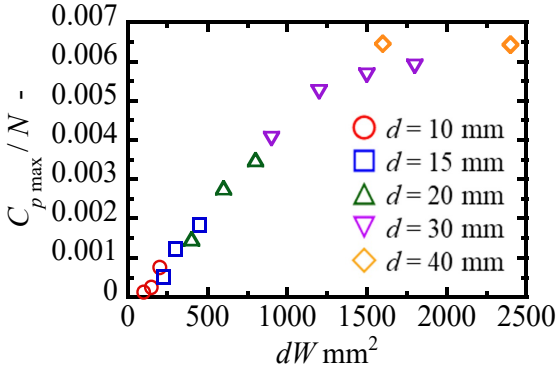

(b) Results restricted to $1 \le W/d \le 2$

Figure 7. Effect of Effective Area of Blade *dW* on Maximum Power Coefficient (*d*=10-40mm, *W*=10-60mm, *D*=155 mm, *L*=220 mm, *s*=4-15 mm, *N*=2, *U*=10m/s).

A load was applied to the wind turbine's rotating shaft using an electromagnetic brake (HB0.5, OGURA CLUTCH Co., Ltd.). The torque T and rotational speed n were measured with a torque meter (UTMII-0.2Nm, Unipulse Co., Ltd.).

3. RESULTS AND DISCUSSION

3.1. Measured toque and evaluated lift force per blade

As shown in Figure 5(a), the torque of this wind turbine increases linearly as the rotational speed decreases when a load is applied to the rotating shaft under a constant mainstream wind speed. Therefore, this torque curve was extrapolated using a linear approximation, and the maximum torque T_{max} was defined as the value obtained when the rotational speed reaches zero. Figure 5(b) illustrates the relationship between the diameter D of the ring plate and T_{max}, while Figure 5(c) presents the relationship between the maximum steady lift force per blade $F_{L\,max}/N$ and D, which was obtained by dividing T_{max} by D. Figure 5(c) indicates that $F_{L\,max}/N$ is nearly independent of D under these conditions.

This suggests that when the cylindrical blade's diameter d and ring width W are sufficiently small, the difference in radius of curvature or circumferential velocity between the inner and outer regions of the ring does not affect the lift, even as the ring diameter D decreases. Additionally, the effect of the vortex generated at the wingtip remains minimal, even if D increases and approaches the wingtip.

Figure 6 shows the maximum steady lift per blade, $F_{L\,max}/N$, when D is varied for an arbitrary combination of d and W. For the d = 10 mm, W = 10 mm combination shown in Figure 5(c), $F_{L\,max}/N$ remained approximately constant regardless of changes in D. However, for the d = 10 mm, W = 15–20 mm combinations, a decrease in $F_{L\,max}/N$ was observed for both large and small values of D. When D is small, the difference in circumferential velocity between the inner and outer diameters of the ring becomes relatively large. Additionally, as D decreases, the size of the hub that supports the rotating shaft and blades remains unchanged, increasing the ratio of flow obstruction to the inner opening area of the ring. These factors contribute to the decrease in $F_{L\,max}/N$ in the small D region.

3.2. Effective area of blade relative to lift

In a cylindrical-blade wind turbine driven by a necklace vortex, the lift force is concentrated near the intersection of the blade and the ring plate. Increasing the blade diameter d and ring width W expands the area over which the lift force acts, leading to a corresponding increase in lift. To quantify this effect, dW is introduced as a new parameter representing the lift-affected area.

Figure 7(a) shows the maximum power coefficient per blade for various combinations of blade diameter d (10 mm to 40 mm) and ring width W (10 mm to 60 mm), obtained by measuring power characteristics. The proportionality to dW does not hold due to performance-interfering phenomena affecting the wind turbine.

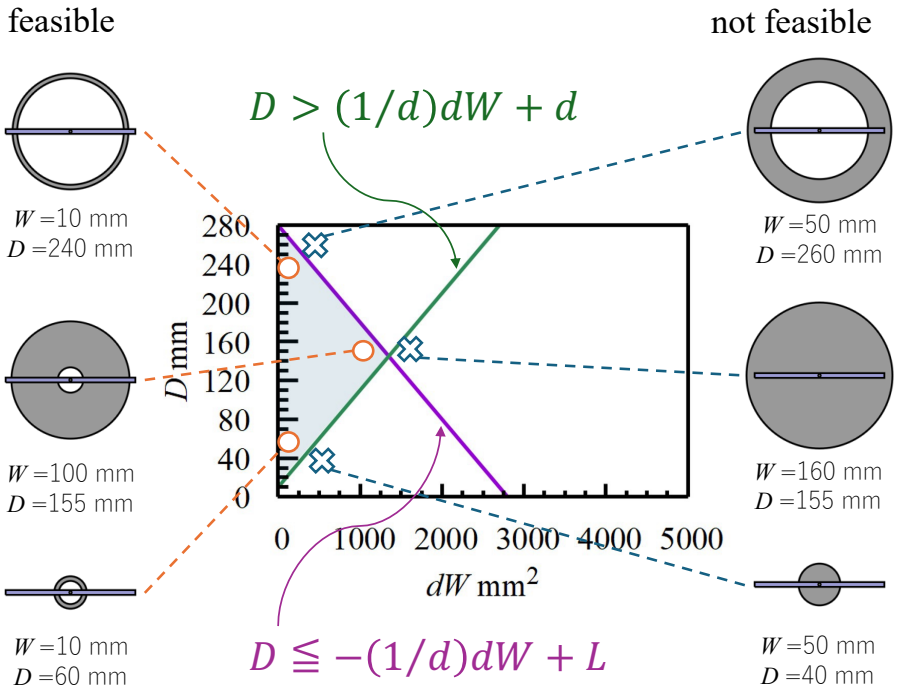

Figure 8. Map illustrating the shape factors required for a viable cylindrical-blade wind turbine.

Figure 7(b) plots a subset of results from Figure 7(a), including only cases where the normalized ring width W/d is between 1 and 2. In this range, the proportional relationship between the power coefficient and dW is maintained across a wide range. This suggests that designing wind turbines within $1 \leq W/d \leq 2$ can help suppress performance-deteriorating effects.

3.3. Conditions for shape factor to be valid as a wind turbine

A cylindrical-blade wind turbine has four shape factors: blade diameter d, blade length L, diameter of ring center D, and ring width W. These factors are not entirely independent, and two constraints must be satisfied to ensure the formation of a necklace vortex and the generation of lift.

The first condition is that the cylindrical blade must not obstruct the inner hole of the ring plate. Since the necklace vortex forms by wrapping around the ring in the direction of its width, a large d with a small D may block the hole, preventing stable vortex formation. Therefore, the inner hole diameter, $D-W$, must be larger than d. Given that dW is used as a design index for wind turbines, this relationship can be expressed as Equation (1).

$$D > (1/d)dW + d \tag{1}$$

The second condition is that the blade must extend beyond the outer edge of the ring. If the blade length L is too short and its tip remains inside the outer diameter of the ring ($D+W$), the necklace vortex will not form. This condition can be expressed as the following equation.

$$D \leqq -(1/d)dW + L \tag{2}$$

For wind turbine design, these conditions are plotted on a plane with the ring plate diameter D on the vertical axis and dW on the horizontal axis, producing the map shown in Figure 8. A wind turbine is geometrically feasible if its parameters fall within the triangular region bounded by the magenta Equation (1) and the green Equation (2). Figure 8 also illustrates examples of wind turbine shapes at characteristic locations both inside and outside this region.

3.4. Distribution of maximum lift force in dW-D map

The maximum lift force of wind turbines with various shapes, measured experimentally, are plotted on the dW-D map in Figure 8. An example is shown in Figure 9, where the color of each point represents the magnitude of the maximum lift coefficient. Additionally, the two blue vertical lines in the figure correspond to W/d=1 and W/d=2. Wind turbines with shapes outside the triangular region defined by Equations (1) and (2) hardly rotated. However, within this triangular region and between the blue vertical lines, the cylinders experienced a stable lift force. Furthermore, within this region, a larger dW results in a higher maximum power coefficient.

4. SUMMARY

In cylindrical-blade wind turbines, which rotate using the lift force from the necklace vortex as the driving mechanism, four key geometric parameters, blade diameter, blade length, ring plate diameter, and ring plate width, were analyzed for their combined effect on power characteristics. Based on these findings, a design guideline was developed to maximize the maximum power coefficient for a given blade length.

REFERENCES

[1] Rashidi, S., Hayatdavoodi M., Abolfazli J., "Vortex shedding suppression and wake control:

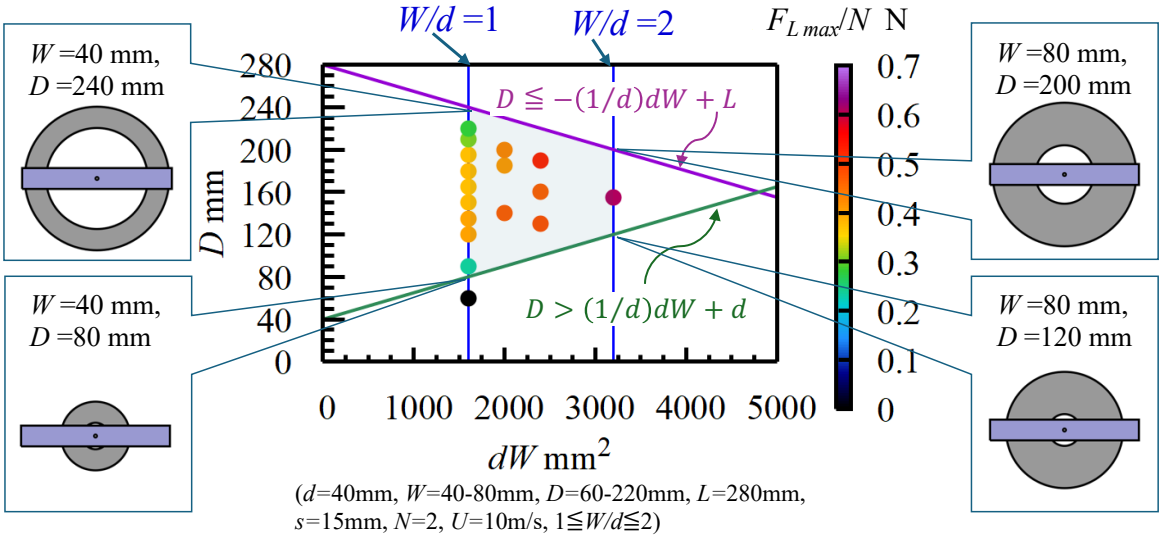

Figure 9. Distribution of the maximum lift force on the *dW-D* map.

a review", Ocean Eng (2016) 126:57–80. https://doi.org/10.1016/j.oceaneng.2016.08.031

[2] Ozono, S., "Vortex suppression of the cylinder wake by deflectors", J Wind E w ng Ind Aerodyn (2003), 91(1–2):91–99. https://doi.org/10.1016/ S0167-6105(02)00337-9.

[3] Hwang, J.Y., Yang, K.S., "Drag reduction on a circular cylinder using dual detached splitter plates", J Wind Eng Ind Aerodyn, (2007), 95(7):551–564. https://doi.org/10.1016/j.jweia.2006.11.003.

[4] Shukla, S., Govardhan, R.N.Ã., Arakeri, J.H., "Flow over a cylinder with a hinged-splitter plate#, J Fluids Struct, (2009), 25(4):713–720. https://doi.org/10.1016/j.jfluidstructs.2008.11.004.

[5] Gozmen, B., Akilli, H., Sahin, B., "Passive control of circular cylinder wake in shallow flow", Measurement, (2013), 46:1125–1136. https://doi.org/10.1016/j.measurement.2012.11.008.

[6] Lee, S-J., Lee, S-I., Park, C-W., "Reducing the drag on a circular cylinder by upstream installation of a small control rod", Fluid Dyn Res (2004) 34:233–250. https://doi.org/ 10.1016/ j.fluiddyn.2004.01.001.

[7] Bae, H.M., Baranyi, L., Koide, M., Takahashi, T., Shirakashi, M., "Suppression of Karman vortex excitation of a circular cylinder by a second cylinder set downstream in cruciform arrangement", J Comput Appl, (2001) Mech 2(2):175–188. https://doi.org/10.1007/s13398-014-0173-7.2.

[8] Kumagai, I., Matsumoto, T., Takahashi, T., Shirakashi, M., "Necklace vortex excitation of upstream cylinder in crisscross circular cylinder system (influence of cylinder diameter, gap and damping factor). JSME Int J Ser B, (2001), 44(4):756–763. https://doi.org/10.1299/jsmeb.44.756.

[9] Kato, N., Koide, M., Takahashi, T., Shirakashi, M, "VIVs of a circular cylinder with a downstream strip-plate in cruciform arrangement. J Fluids Struct 30:97–114. https://doi.org/10.1016/j.jfluidstructs.2012.02.007.

[10] Koide, M., Sekizaki, T., Yamada, S., Takahashi, T., Shirakashi, M., "Prospect of micro power generation utilizing VIV in small stream based on verification experiments of power generation in water tunnel", J Fluid Sci Technol, (2013), 8(3):294–308. https://doi.org/10.1299/jfst.8.294

[11] Sakamoto, K., Hemsuwan, W. and Takahashi, T., "Development of circular cylinder blade wind turbine driven by longitudinal vortex", Transactions of the JSME (in Japanese), Vol. 87, No.894 (2021), pp. 20-00365

[12] Sakamoto, K., Hemsuwan, W. and Takahashi, T., "Numerical investigation of lift-force generation on a moving circular cylinder in a uniform flow driven by longitudinal vortex", Journal of Fluids and Structures, Vol. 83, (2018), pp. 448-470

[13]Sakamoto, K., Hemsuwan, W. and Takahashi, T., "Development of a wind turbine driven by longitudinal vortex: Wind tunnel experiment to investigate the basic characteristics of the wind turbine using a single circular cylinder blade", Journal of Wind Engineering and Industrial Aerodynamics, Vol.210 (2021), pp.104492